

Probing Dark Matter and Dark Energy with Space-Based Weak Lensing

Richard Massey

Institute of Astronomy, Madingley Road, Cambridge CB3 0HA, UK

Alexandre Refregier

Service d'Astrophysique, CEA/Saclay, 91191 Gif sur Yvette, France

Jason Rhodes

California Institute of Technology, 1201 E. California Blvd., Pasadena, CA 91125, USA

Abstract.

Weak lensing provides a direct measure of the distribution of mass in the universe, and is therefore a uniquely powerful probe of dark matter. Weak lensing can also be used to measure the twin phenomenon of dark energy, via its effect upon the cosmological growth rate of structures. Essential for this technique are well-resolved images of background galaxies out to large distances. As a concrete example of the surveys that will become available by the end of the decade, we consider the planned *Supernova/Acceleration Probe* (SNAP) space telescope. Detailed simulations of space-based images, manufactured using the shapelets formalism, enable us to quantitatively predict the future sensitivity to weak lensing shear. The high number density of galaxies resolved from space will enable maps of dark matter to be produced in two and three dimensions, with a resolution superior to that from the ground. Such observations will also afford reduced systematics for high-precision measurements of weak lensing statistics. These will be used to set tight constraints on cosmological parameters. In particular, the parameter for equation of state of dark energy, w , will be measured using weak lensing with a precision comparable to and somewhat orthogonal to constraints from other methods.

1. Introduction

During its journey to our telescopes, the light from background galaxies is deflected by foreground mass concentrations, which act as gravitational lenses along the line-of-sight. The observed distortions in the shapes of distant galaxies are directly related to the gravitational potential of foreground structures, and therefore to their mass. This effect is independent of the nature or state of the foreground mass and therefore traces the distribution of otherwise invisible

dark matter. In recent years, many groups have measured coherent distortions in the shapes of galaxies to measure the mass distribution of clusters (*e.g.* Joffre *et al.* 2000; Clowe, Trentham & Tonry 2001; Dahle *et al.* 2002). Other groups have measured the distribution of large-scale structure in random regions in the sky to set constraints on cosmological parameters (*e.g.* van Waerbeke *et al.* 2002; Bacon *et al.* 2002; Hoekstra *et al.* 2002; Jarvis *et al.* 2003). The second moment of the resulting “cosmic shear” field already provides a constraint on the amplitude of the mass power spectrum $\Omega_m \sigma_8^{0.5}$ which is comparable to the constraints set by more traditional methods such as the abundance of x-ray selected clusters (*e.g.* Viana & Liddle 1999; Pierpaoli, Scott & White 2001). The higher order moments of the shear field promise to break the Ω_m - σ_8 degeneracy (Bernardeau *et al.* 1997) in the next generation of large cosmic shear surveys, *e.g.* CFHT Legacy Survey (CFHTLS, Mellier *et al.* 2000), LSST (Tyson *et al.* 2002a) and Pan-STARRS (Kaiser, Tonry & Luppino 2000). For reviews of the techniques and current status of weak lensing measurements, other than this volume, see Mellier *et al.* (2001), Hoekstra *et al.* (2002), Wittman (2002) and Refregier (2003).

The rapid growth of dedicated surveys and improvements in shear measurement methods has meant that errors on cosmological parameters from cosmic shear are now limited by systematic rather than statistical errors. Weak lensing has the advantage that its systematics arise from imperfect instruments and image analysis, rather than unknown physics (such as the mass-temperature relation which dominates x-ray selected cluster samples (Huterer & White, 2002)). Image analysis tools are currently making important advances, from the well-tested method of Kaiser, Squires & Broadhurst (1995; KSB), with work by Rhodes, Refregier & Groth (2000; RRG), Bernstein & Jarvis (2003) and “shapelets” by Refregier (2003a). Meeting the engineering challenge, however, will inevitably require rising above the atmosphere. Convolution with a large Point-Spread Function (PSF) that is larger than the majority of distant (and therefore small) objects irretrievably destroys any information their shapes had contained. This limits the number density and redshift of galaxies that can be used to measure cosmic shear with ground-based lensing surveys. Convolution with the time-varying atmospheric PSF further limits the recovery of the shape information of the remaining galaxies to the accuracy with which the PSF can be modelled from one exposure to the next.

In these proceedings, we discuss the potential advances that a wide-field imager from space offers for weak lensing. Adopting the planned *Supernova/Acceleration Probe* (SNAP) mission as a concrete example, we present detailed shapelet-based simulations used to estimate the lensing sensitivity of such observations. Most interestingly for cosmology, SNAP’s enhanced spatial resolution will capture the shapes of background galaxies up to a much greater distance. Space-based surveys will therefore probe the evolution of the mass distribution, and the growth of structures, over a large fraction of time in the evolution of the universe. This evolution provides strong constraints on both Ω_m and the equation of state parameter of dark energy w . As discovered from observations of type Ia supernovæ (*e.g.* Perlmutter *et al.* 1999), this dark energy or “quintessence” is accelerating the expansion of the universe and hence retarding the growth of the mass power spectrum. Earlier studies of the constraints on dark energy from weak lensing surveys can be found in Hu (1999), Huterer

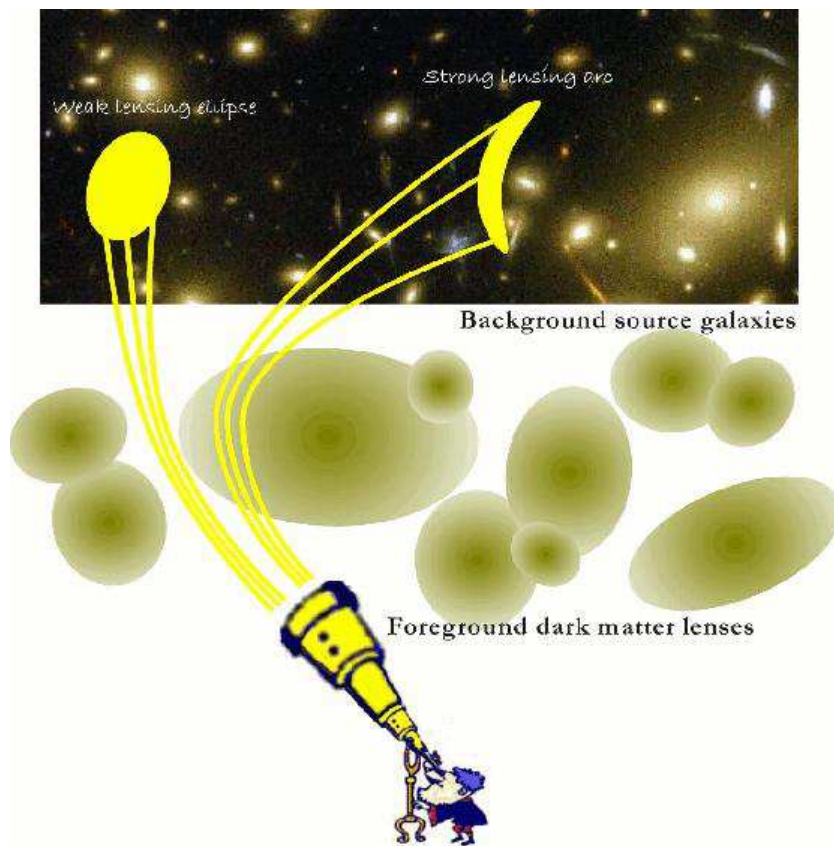


Figure 1. Illustration of the effect of gravitational lensing. Foreground dark matter haloes differentially shear the light paths from background galaxies, distorting their shapes into an ellipse (when averaged over many galaxy shapes) or arcs near the centres of clusters.

(2001), Benabed & Bernardeau (2001), Hu (2001), Weinberg & Kamionkowski (2002), Munshi & Wang (2002), Benabed & van Waerbeke (2003). We also compare the quality of dark matter maps that will be possible from SNAP with those possible from current ground-based surveys. High resolution maps from space will enable the production of a fully mass-selected cluster catalogue, useful for a further constraint on cosmological parameters (Miyazaki *et al.* 2002) but also for investigations into astrophysical effects during the non-linear infall and growth on smaller scales. Full details of our calculations are given in a series of papers by Rhodes *et al.* (2004), Massey *et al.* (2004b) and Refregier *et al.* (2004b).

2. Principles of Weak Lensing

Gravitational lensing subjects the apparent images of background galaxies to a distortion that is characterized by the distortion matrix (see Figure 1 for an illustration, and Bartelmann & Schneider 1999 for a detailed review)

$$\Psi_{ij} \equiv \frac{\partial(\delta\theta_i)}{\partial\theta_j} \equiv \begin{pmatrix} \kappa + \gamma_1 & \gamma_2 \\ \gamma_2 & \kappa - \gamma_1 \end{pmatrix}, \quad (1)$$

where $\delta\theta_i(\theta)$ is the deflection vector produced by lensing on the sky. The convergence κ describes overall dilations and contractions, and is proportional to the projected mass along the line of sight. The shear γ_1 (γ_2) describes stretches and compressions along (at 45° from) the x -axis.

The distortion matrix is directly related to the matter density fluctuations along the line of sight by

$$\Psi_{ij} = \int_0^{\chi_h} d\chi g(\chi) \partial_i \partial_j \Phi, \quad (2)$$

where Φ is the Newtonian potential, χ is the comoving distance, χ_h is the comoving distance to the horizon, and ∂_i is the comoving derivative perpendicular to the line of sight. The radial weight function $g(\chi)$ reflects the fact that a lens is most effective when placed approximately half-way between the source and the observer. It is given by

$$g(\chi) = 2 \int_\chi^{\chi_h} d\chi' n(\chi') \frac{r(\chi)r(\chi' - \chi)}{r(\chi')}, \quad (3)$$

where r is the comoving angular-diameter distance. The function $n(\chi)$ is the distribution of the galaxies as a function of the comoving distance χ from the observer and is assumed to be normalized as $\int d\chi n(\chi) = 1$.

Galaxies have an intrinsic distribution of shapes, but distant ones are randomly oriented in the absence of lensing. When a shear is applied to the galaxies in a particular patch of the sky, they become coherently distorted and their average shape changes from a circle to an ellipse. This observed ellipticity can be converted into the applied shear using a method like KSB, which properly takes into account their size distribution and radial profiles. Thus the cosmic shear field is an observable. By inverting the lensing equation (eqn. 2), the shear map can be converted into a map of the projected mass κ and, therefore, of the dark matter distribution.

3. Cosmological models with Dark Energy

We consider a cosmological model with a matter component and a dark energy (or ‘‘quintessence’’) component with present density parameters Ω_m and Ω_q , respectively. The equation of state of the dark energy is parametrized by $w = p_q/\rho_q$, which we assume to be constant and is equal to -1 in the case of a cosmological constant. The evolution of the expansion parameter a is given by the Hubble constant H through the Friedmann equation

$$H = \frac{\dot{a}}{a} = H_0 \left(\Omega_m a^{-3} + \Omega_q a^{-3(1+w)} + \Omega_\kappa a^{-2} \right)^{\frac{1}{2}}, \quad (4)$$

where $\dot{a} = da/dt$ and the total and curvature density parameters are Ω and $\Omega_\kappa = 1 - \Omega$, respectively. The present value of the Hubble constant is parametrized as $H_0 = 100h \text{ km s}^{-1} \text{ Mpc}^{-1}$.

As a reference model, we consider a fiducial Λ CDM cosmology with parameters $\Omega_m = 0.30$, $\Omega_b = 0.047$, $n = 1$, $h = 0.7$, $w = -1$, consistent with the recent CMB measurements from the WMAP experiment (Spergel *et al.* 2003). In agreement with this experiment, we assume that the universe is flat, *i.e.* that $\Omega = \Omega_m + \Omega_q = 1$.

Dark energy has several effects on weak lensing statistics (Ma *et al.* 1999). First, it modifies the expansion history of the universe $a(t)$. As a result, both the angular-diameter distance and the growth rate of structures are modified. The latter effect is amplified by the non-linear evolution of structures. In some quintessence models, dark energy also modifies the linear power spectrum on large scales. We will ignore that effect since these scales are not easily probed by weak lensing surveys.

4. Cosmic shear statistics

The properties of the cosmic shear field can be quantified by several statistics. The most basic statistic is the weak lensing power spectrum. This is the equivalent in Fourier space of the shear-shear correlation functions, and is given by (*e.g.* Bartelmann & Schneider 1999; Hu & Tegmark 1999; see Bacon *et al.* 2001 for conventions)

$$C_\ell = \frac{9}{16} \left(\frac{H_0}{c} \right)^4 \Omega_m^2 \int_0^{\chi_h} d\chi \left[\frac{g(\chi)}{ar(\chi)} \right]^2 P\left(\frac{\ell}{r}, \chi\right), \quad (5)$$

where $r(\chi)$ is the comoving angular diameter distance, and χ_h corresponds to the comoving radius to the horizon. Considerable uncertainties remain for the non-linear power spectrum $P(k, z)$ in quintessence models (see discussion in Huterer 2001). Here, we will use the prescription of Peacock & Dodds (1996) to evaluate it from the linear power spectrum. The growth factor and COBE normalization for arbitrary values of w can be computed using the fitting formulæ from Ma *et al.* (1999).

The left-hand panel of figure 2 shows lensing power spectra for the fiducial Λ CDM model with background galaxies in two different shells, with median redshifts of 0.96 and 1.73. Deviations from the model are also shown, corresponding to variations in Ω_m and w . All models shown are COBE normalised. Note that non-linear corrections are dominant for $\ell \gtrsim 100$.

Non-linear gravitational instability is known to produce non-Gaussian features in the cosmic shear field. The power spectrum therefore does not contain all the information available from weak lensing. We consider the most common measure of non-Gaussianity, namely the skewness S_3 which is defined as (*e.g.* Bernardeau *et al.* 1997)

$$S_3(\theta) \equiv \frac{\langle \kappa^3 \rangle}{\langle \kappa^2 \rangle^2}, \quad (6)$$

where κ is the convergence which can be derived from the shear field γ_i and the angular brackets denote averages over circular top-hat cells of radius θ . The denominator is the square of the convergence variance which is given by

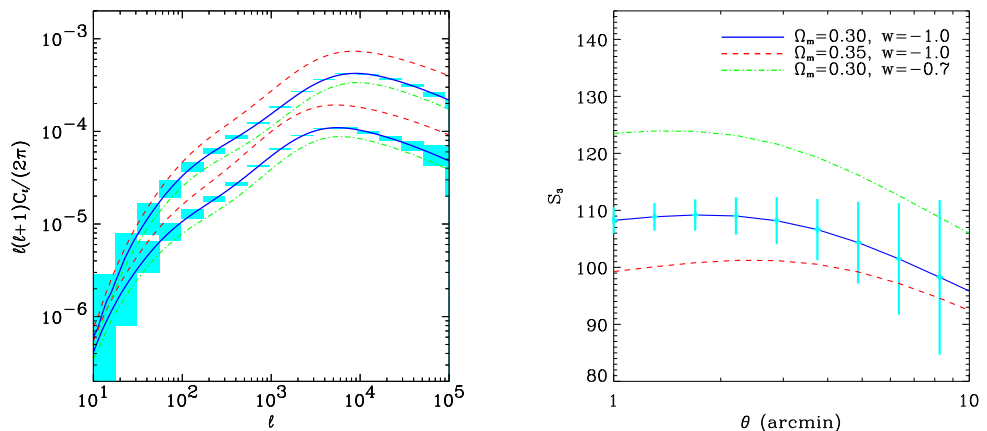


Figure 2. Weak lensing statistics for different cosmological models. Variations of 17% in Ω_m and of 30% in w about the fiducial Λ CDM model are displayed. Left: the weak lensing power spectrum C_l for two galaxy samples with median redshifts of 0.96 and 1.73. Right: skewness S_3 of the convergence κ as a function of scale θ . In each case, the expected band-averaged 1σ error bars for the SNAP weak lensing surveys are shown as blocks. (Adapted from Refregier *et al.* 2004b).

$$\langle \kappa^2 \rangle = \langle \gamma^2 \rangle \simeq \frac{1}{2\pi} \int d\ell \ell C_\ell |W_\ell|^2, \quad (7)$$

where $W_\ell \equiv 2J_1(\ell\theta)/(\ell\theta)$ is the window function for such cells and C_ℓ is the lensing power spectrum given by equation (5). To evaluate the numerator $\langle \kappa^3 \rangle$ of equation (6), we use the approximation of Hui (1999) who used the Hyper-extended perturbation theory of Scoccimarro & Frieman (1999). While more accurate approximations for third order statistics now exist (see van Waerbeke *et al.* 2001 and references therein), the present one suffices for our present purpose.

The right-hand panel of figure 2 shows the skewness as a function of scale for the same cosmological models considered in the left-hand panel. The skewness is only weakly dependent on the angular scale θ , but depends more strongly on Ω_m and w .

5. SNAP: a wide field imager from space

The *Supernova/Acceleration Probe* (SNAP) satellite has a planned launch date in 2010. The latest design of this wide-field 2m space telescope is shown in figure 3. Many of the stringent optical requirements for following the light curves of faint supernovae are compatible with the desired instrumental properties for measurements of weak lensing. Indeed, most of SNAP's limitations and trade-offs will be born by any similar wide-field imager from space. The detailed engineering models which are available for SNAP therefore act as a useful base-



Figure 3. Cutaway view of the proposed SNAP satellite design, showing the internal light baffles, the 2m primary mirror and the three sturdy support struts of the secondary mirror. The solar panels are fixed to the outside on one side of the craft, with a radiator in the opposite direction. Their orientation with respect to the sun is permanently maintained in order to minimise thermal expansions and contractions that would otherwise induce optical distortions, mimicking lensing shear. Image reproduced courtesy of the SNAP collaboration.

line for a generic space mission which will inevitably face similar engineering difficulties and reach similar solutions.

SNAP's 0.7 square degree field of view will be covered by a mosaic of nine fixed filters spanning the optical and near IR from 350nm–1.7 μ m (Perlmutter *et al.* 2003). These are arranged in such a pattern that scanning the telescope horizontally or vertically across the sky will build up an image of a contiguous survey region in all nine bands. At 800nm, the FWHM of the PSF will be approximately 0.15". The PSF, and any internal optical distortion (that could mimic cosmic shear), will remain stable because of the satellite's high and therefore thermally stable orbit. Indeed, the telescope will rarely enter the shadow of the Earth and always maintain the same face pointing towards the sun (Rhodes *et al.* 2004).

The SNAP survey strategy is divided into two primary missions. A deep survey to ABmag 30.2 in R (for a point source at 5σ), will cover 15 square degrees in all nine bands. This will be built up over a period of 32 months, by stacking observations taken once every four days in a search for type Ia supernovae light curves. A second, wide survey to ABmag 27.7 will cover 300 square degrees. This will be gathered during a period of 5 months.

Two major weak lensing applications are enabled by the SNAP mission. The high number density of resolved galaxies ($\gtrsim 250$ arcmin $^{-2}$) in the deep survey will be uniquely useful to construct high-resolution mass maps and search for galaxy clusters by mass. Complementing this, the wide survey is essential to

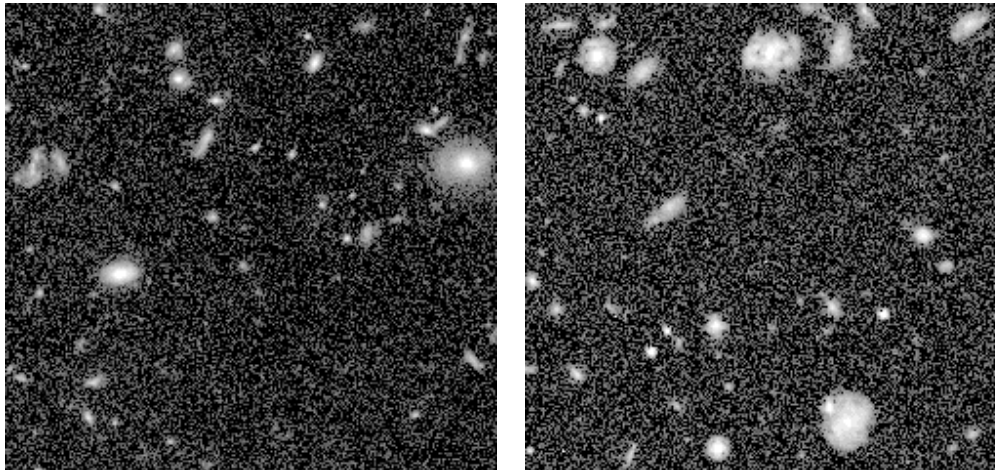


Figure 4. An example of the realistic simulated images created using the shapelet method of Massey *et al.* (2004a). The left panel shows a $30' \times 30'$ section of the real HDF. The right panel shows a section of a simulated image with the same size and scale. The galaxies it contains are no longer simple parametric models, but instead possess complex morphologies that are statistically similar to those in observed data. (Adapted from Massey *et al.* 2004a).

reduce the impact of cosmic variance on cosmological parameter estimation. For this purpose, it is important that relatively high redshifts can still be reached in even a modest exposure time from space – and with sufficient colours, including near IR, to provide accurate photometric redshifts.

6. Shapelet-based image simulations

The image simulation method of Massey *et al.* (2004a) was developed to mimic deep, high resolution space-based data. The simulations use the “shapelets” formalism of Refregier (2003a) to create realistic galaxies of all morphological types and with all the substructure and irregularity of faint HDF objects. The simulated objects possess a known size, magnitude and input shear, and may be used to calibrate the sensitivity of an instrument to weak lensing.

As a specific case, we have manufactured simulated images to the design specifications of the SNAP satellite. Since an object’s response to shear is a function of its overall shape, the presence of realistic and irregular galaxy morphologies is an important advance over earlier work (Bacon *et al.* 2001, Erben *et al.* 2001), which had used only azimuthally symmetric simulated galaxies with radial profiles parametrized as de Vaucouleurs $r^{1/4}$ laws or exponential discs. $30' \times 30'$ sections of an example simulated image and a similarly scaled section of the HDF are shown in figure 4.

To generate the image, the galaxies in the HDF-North and HDF-South are first decomposed into shapelets. Shapelets are a complete basis set of two-dimensional, orthonormal basis functions, constructed from Laguerre functions

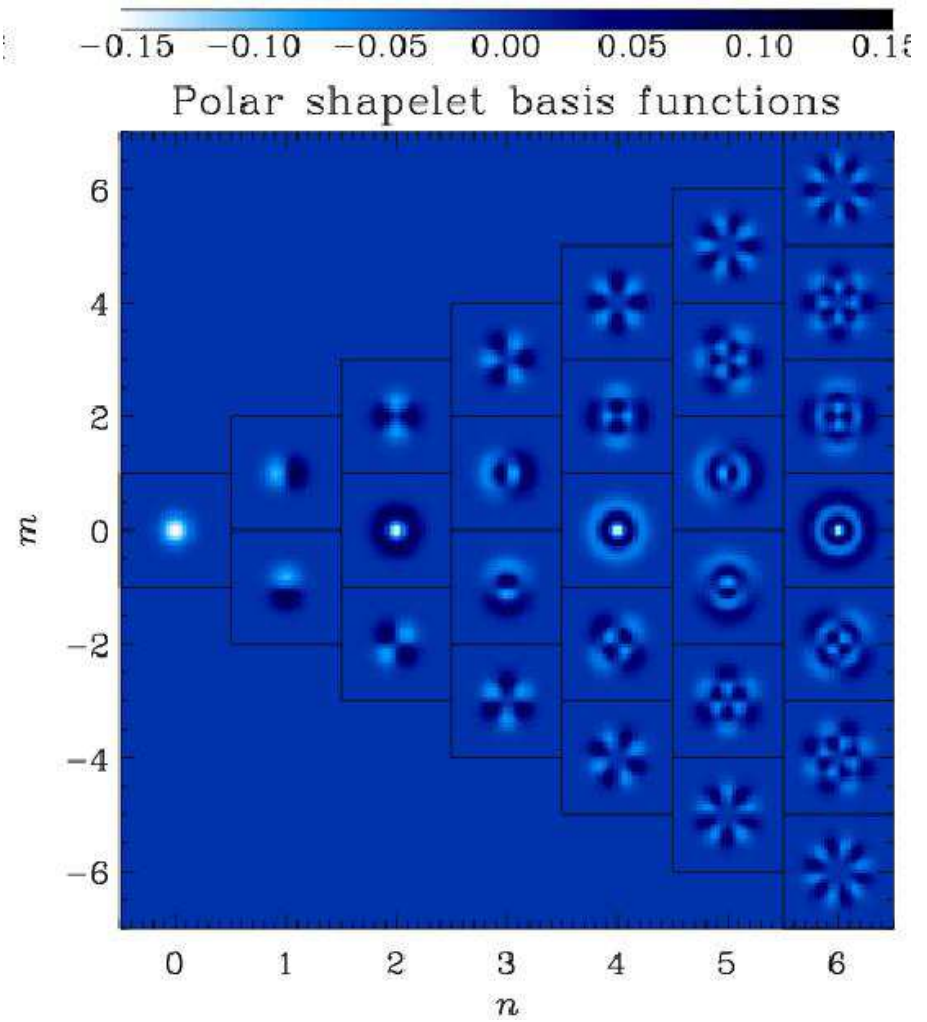


Figure 5. Polar shapelet basis functions. These are a complete, orthonormal basis set with which galaxy shapes can be modelled and regenerated later. Shapelets are mathematically convenient for many aspects of image analysis and lie at the core of the image simulation method.

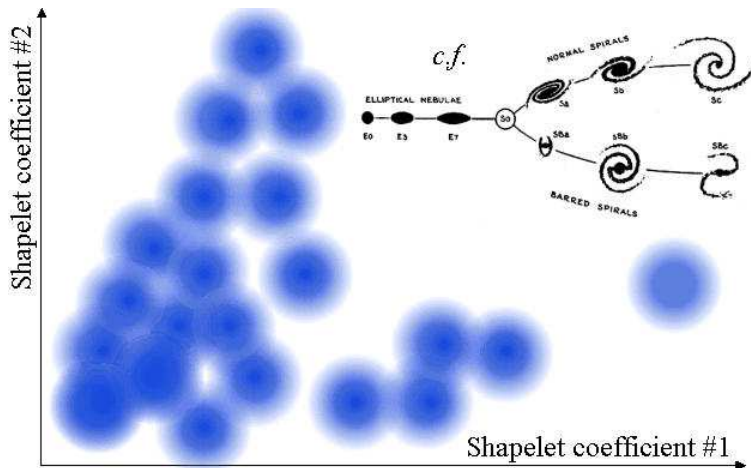


Figure 6. Idealised representation of a slice through shapelet morphology parameter space, where each dimension corresponds to a shapelet coefficient. The points represent the position of an observed HDF galaxy in shapelet space. Their distribution encode the underlying morphology distribution of real galaxies, like a multi-dimensional Hubble sequence. This morphology distribution can be smoothed and resampled to generate an unlimited number of unique, yet realistic galaxy shapes for the image simulations.

multiplied by a Gaussian, as shown in figure 5. This basis is mathematically convenient for many aspects of image manipulation and analysis, including weak lensing shear and magnification. Linear combinations of shapelet basis states, weighted by “shapelet coefficients”, can be used to model any localised shape, rather like Fourier or wavelet synthesis. The shapelet coefficients are Gaussian-weighted multipole moments of the object, which can be used for quantitative shape measurement.

The shapelet coefficients of the real HDF galaxies populate an n -dimensional vector space, where n is the maximum number of coefficients used. The vector space is illustrated in figure 6. It is analogous to the Hubble tuning fork: some regions of shapelet space represent spiral galaxies; other regions represent early-type elliptical galaxies. The underlying distribution of galaxy morphologies is only finitely sampled by the HDF, but may be recovered by smoothing the distribution in shapelet space. Massey *et al.* (2004a) justify this process by comparing SExtractor and concentration/asymmetry morphology estimators of real data to the consistent statistics of shapelet-generated galaxies in the final simulated images.

An image of distant galaxies can then be manufactured by repeatedly resampling the recovered morphology distribution. Figure 7 illustrates the steps taken to produce a realistic simulated image. These steps mimic the processes acting on photons en route from a distant galaxy to a telescope. First, the galaxies are sheared by the input gravitational lensing signal. Then they are convolved with the SNAP PSF and slightly distorted through a model of the telescope’s internal optics. Typical observational noise is added at the end. These images

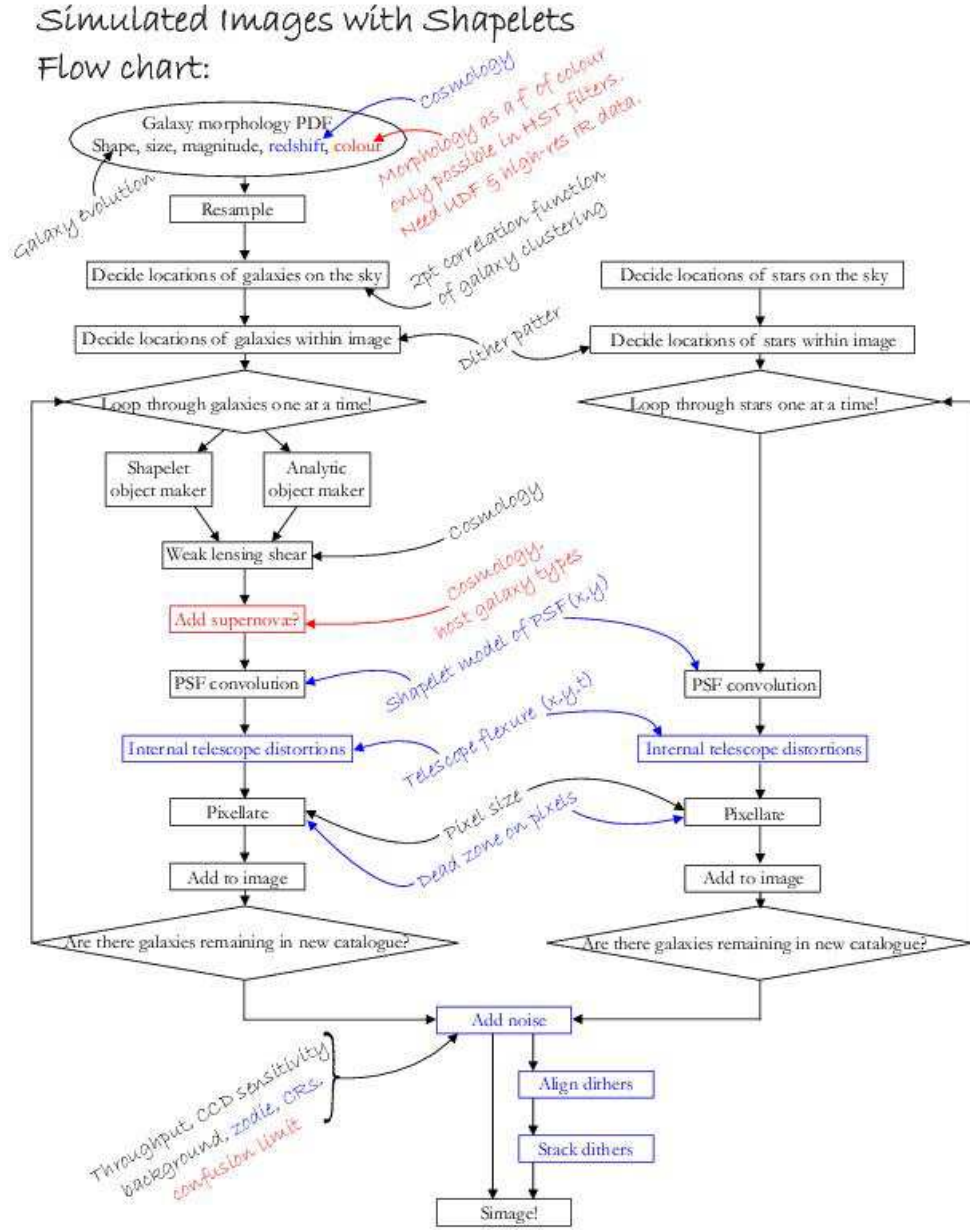


Figure 7. Flowchart showing the steps taken to produce a simulated image. These steps mimic the processes acting on photons en route from a distant galaxy to a telescope. The required inputs from cosmology, an engineering model of the telescope and a survey strategy are shown in a script font. Type Ia supernovae could also be added, to simulate the other aspect of the SNAP mission.

can then be fed into a data reduction and shear measurement pipeline. As we show in the next section, comparing the known input shear with the output of this pipeline helps both to determine SNAP’s sensitivity to weak lensing and to calibrate and improve shear measurement algorithms.

7. Weak Lensing Measurement

We have used the RRG shear measurement method to attempt to recover the known level of shear input to the simulated images. Figure 8 shows the sensitivity to shear as a function of exposure time.

There are three main advantages of using space-based images for weak lensing measurements. Firstly, the smaller PSF means that there is a higher space density of galaxies sufficiently resolved for their shears to be measured, and shot noise is reduced on small scales. This is illustrated in the top panel of figure 8. Although the number of *detected* galaxies (dotted line) increases rapidly with increasing exposure time, the fraction of these which are resolved (solid line) begins to drop as the size distribution of the faint galaxies falls beneath the PSF size. Note that the simulations currently extend only to the depth of the HDF. The slope of the number counts beyond this, and the shape properties of these faint galaxies are unknown. We therefore await deeper observations with the ACS to probe this regime.

The second advantage of space is that the galaxies resolved from space are generally further away than those just resolved from the ground. The cosmic shear signal is predicted to increase with survey depth due to the cumulative lensing by more structures along the line of sight. The middle panel of figure 8 shows a prediction of the mean redshift of galaxies in the lensing sample as a function of exposure time. This is calculated via a simple model of median magnitude *vs* median z , extrapolated from photometric observations of the HDF (Lilly *et al.* 1996).

The third advantage is that the shape of each galaxy can be more reliably measured. Not only is the S/N higher on each galaxy, with more resolved morphological detail, but the correction for instrumental smearing and distortion can be much more accurate because of SNAP’s stable PSF. The PSF stability of SNAP will be superior even to that of HST, which suffers from telescope breathing due to the large changes in its temperature while passing in and out of direct sunlight during each orbit.

The bottom panel of figure 8 shows the resulting sensitivity to lensing of a space-based mission like SNAP. The error on the shear of galaxies binned into 1 arcmin² patches on the sky is shown as a function of exposure time. The dotted line shows the expected cosmic shear signal, which increases with exposure time due to the cumulative lensing by more and more objects as the survey depth increases. The S/N on scales of 1 arcmin² is about 1 and greater than about 1.8 for the wide and deep surveys respectively. As we discuss in the next section, this offers great prospects for mapping the dark matter.

In contrast to this precision from space, consider the limitations from a ground-based telescope. The ESI camera on Keck has proven itself to have minimal levels of internal optical distortion and telescope flexure, as required for high precision weak lensing measurements. The size of the primary mirror also

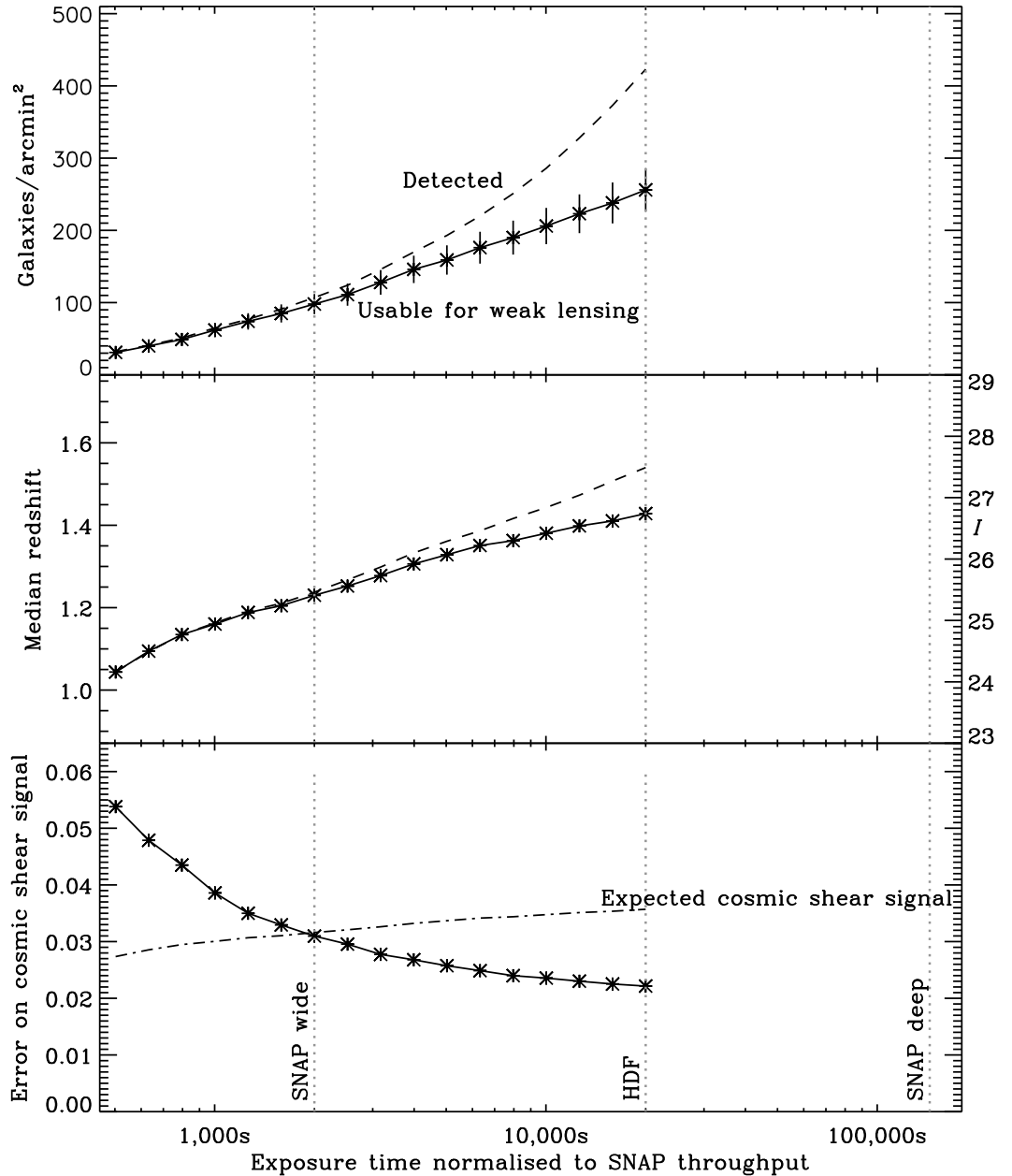


Figure 8. Sensitivity to weak lensing shear, as a function of exposure time on SNAP. Deep ACS images are awaited to model galaxies fainter than the current limit of the HDF. Top panel: the number density of detected objects (dashed) and of the subset sufficiently well resolved to be useful for shear measurement (solid). Middle panel: the increase in redshift as a function of survey depth for the two galaxy populations shown above. Bottom panel: the predicted error on cosmic shear measurements in bins of 1 arcmin^2 , using SNAP. Shown dotted is the prediction of cosmic shear signal for a Λ CDM model. On $1'$ scales, the SNAP wide survey will achieve an average S/N of unity: ideal for making maps. (Adapted from Massey *et al.* 2004b).

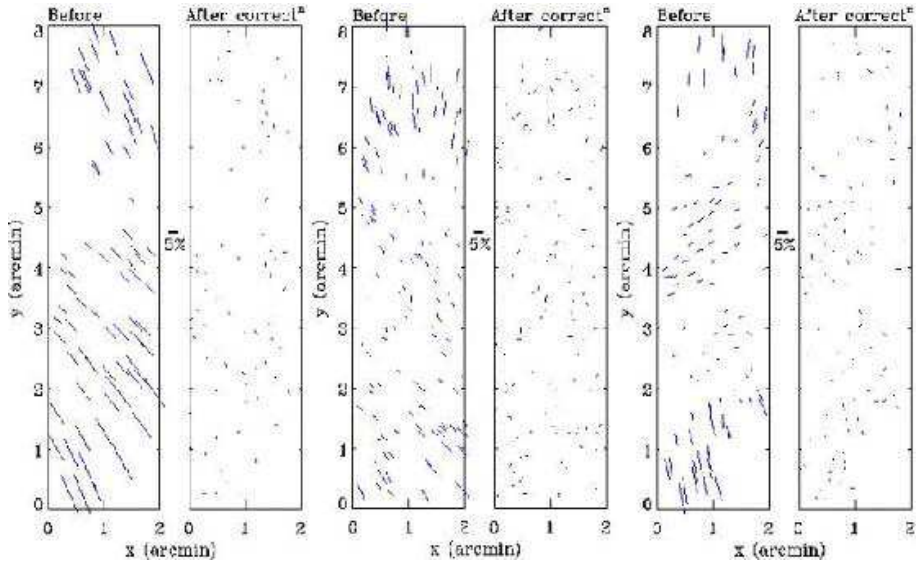


Figure 9. The constantly changing PSF anisotropy patterns from one night on Keck. Although systematics effects are well-controlled on Keck, and exposure times can be short, the seeing effects of the atmosphere are unavoidable. Shown above are the amount and direction of PSF ellipticities as measured from stars, before and after corrections. The patterns are not well understood but are probably due to a combination of imperfect tracking, telescope flexure, and atmospheric turbulence. The galaxy shapes must be corrected for these effects before shear measurements can be achieved. Plotted on the same scale, the equivalent PSF ellipticities for SNAP would be barely visible.

lets it reach useful depths in exposures of only ten minutes (Bacon *et al.* 2002). However, even in this short time, variations in the ground-based PSF seriously affect weak lensing observations with any ground-based telescope. Figure 9 shows examples of these changing atmospheric patterns, all taken with ESI on the same night. The line segments show the direction and ellipticity of the PSF, as measured from stars. Bacon *et al.* (2001) and Erben *et al.* (2001) demonstrated that the smearing of object shapes can be corrected at a level of $\sim 90\%$ using the KSB method, and the corrected shapes of our stars are also shown in figure 9.

From space, the raw PSF ellipticities before correction are around the level on Keck after correction (Rhodes *et al.* 2004). Coupled with more stable optics, and newer correction methods, this will result in a reduction in overall systematic contamination by at least an order of magnitude.

8. Cosmological constraints

Two- and three-point statistics of the cosmic shear field in the wide SNAP survey will be used to constrain cosmological parameters. Figure 2 shows the effect of

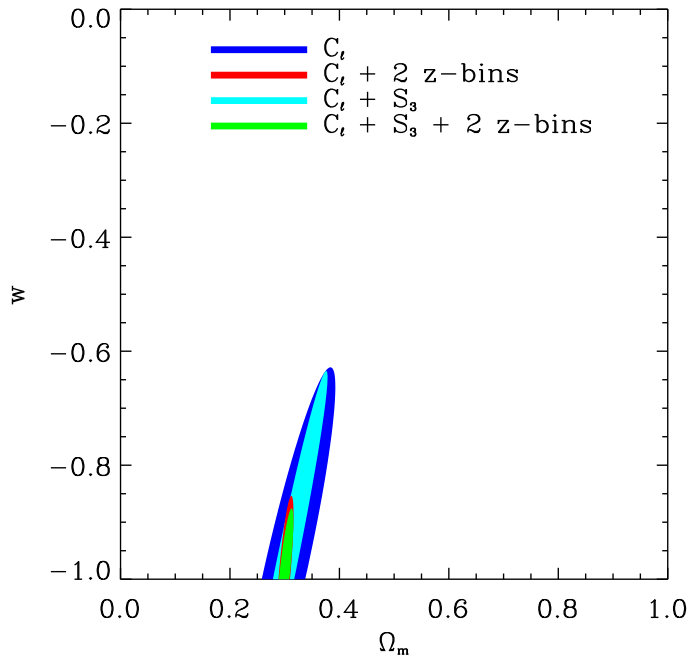


Figure 10. Predicted cosmological parameter constraints from SNAP weak lensing (Refregier *et al.* 2004b). Contours show 68% CL limits constraints derived from the power spectrum C_l using the SNAP wide survey ($A = 300 \text{ deg}^2$, $\sigma_\gamma = 0.31$ and $n_g = 100 \text{ deg}^{-2}$). From top to bottom, the different colours show constraints with and without photometric redshifts, with the skewness S_3 and with all of them combined. A COBE normalisation prior was used. (From Refregier *et al.* 2004b).

varying Ω_m and w on the weak lensing power spectrum and skewness. The lensing power spectrum is shown for 2 bins of galaxy redshifts which can be derived from photometric redshifts. The error bars expected for the SNAP wide survey (using $A = 200 \text{ deg}^2$, $\sigma_\gamma = 0.31$ and $n_g = 100 \text{ deg}^{-2}$) are displayed. The excellent precision afforded by SNAP will easily distinguish the models shown, and thus detect small changes in the properties of dark energy (Refregier *et al.* 2004b).

We can compute the constraints which can be set on cosmological parameters using the Fisher matrix (*e.g.* Hu & Tegmark 1999)

$$F_{ij} = - \left\langle \frac{\partial \ln \mathcal{L}}{\partial p_i \partial p_j} \right\rangle, \quad (8)$$

where \mathcal{L} is the Likelihood function, and p_i is a set of model parameters. The inverse \mathbf{F}^{-1} provides a lower limit for the covariance matrix of the parameters.

Figure 10 shows the constraints on the Ω_m - w plane that will be possible from SNAP. The measurement of the weak lensing power spectrum at two differ-

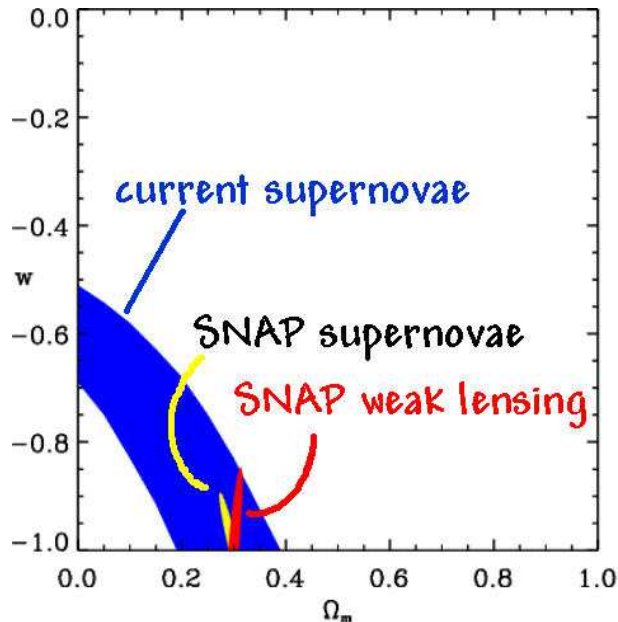


Figure 11. A comparison of the constraints derived from weak lensing with SNAP (using the combined skewness and tomography statistics as before, but without the COBE prior), from that with current and future SNAP supernova surveys (Perlmutter *et al.* 1999, 2003). (Adapted from Refregier *et al.* 2004b).

ent redshifts (or “redshift tomography”) provides an important lever arm upon the growth of structure and the evolution of the power spectrum, improving the constraints significantly. The addition of the skewness (at a single angular scale) does not improve the constraints as much. Figure 11 compares the constraints from weak lensing (using the power spectrum in two redshift bins and the skewness) to that which can be derived from current and the future SNAP supernova surveys (Perlmutter *et al.* 1999, 2003). Note however that the supernovae constraints shown include systematic errors and a marginalisation over w' , the time derivative of w . The SNAP weak lensing survey will therefore provide constraints on the dark energy which are comparable with and complementary to those from the SNAP supernova survey.

9. Dark Matter Mapping

From the observed shear field, one can reconstruct maps of the lensing convergence κ , which is proportional to the total mass projected along a given line of sight. The resolution of the maps depends on the size of the spatial element within which shear or convergence can be accurately measured to a $S/N \sim 1$. The SNAP wide survey has been tailored to resolve the shapes of ~ 100 background galaxies per square arcminute, over 300 square degrees. For the instrumental sensitivity to shear read from figure 8, this will achieve maps with a resolution of 1 arcmin² pixels (~ 250 kpc at $z = 0.3$). Extrapolating our simulations beyond

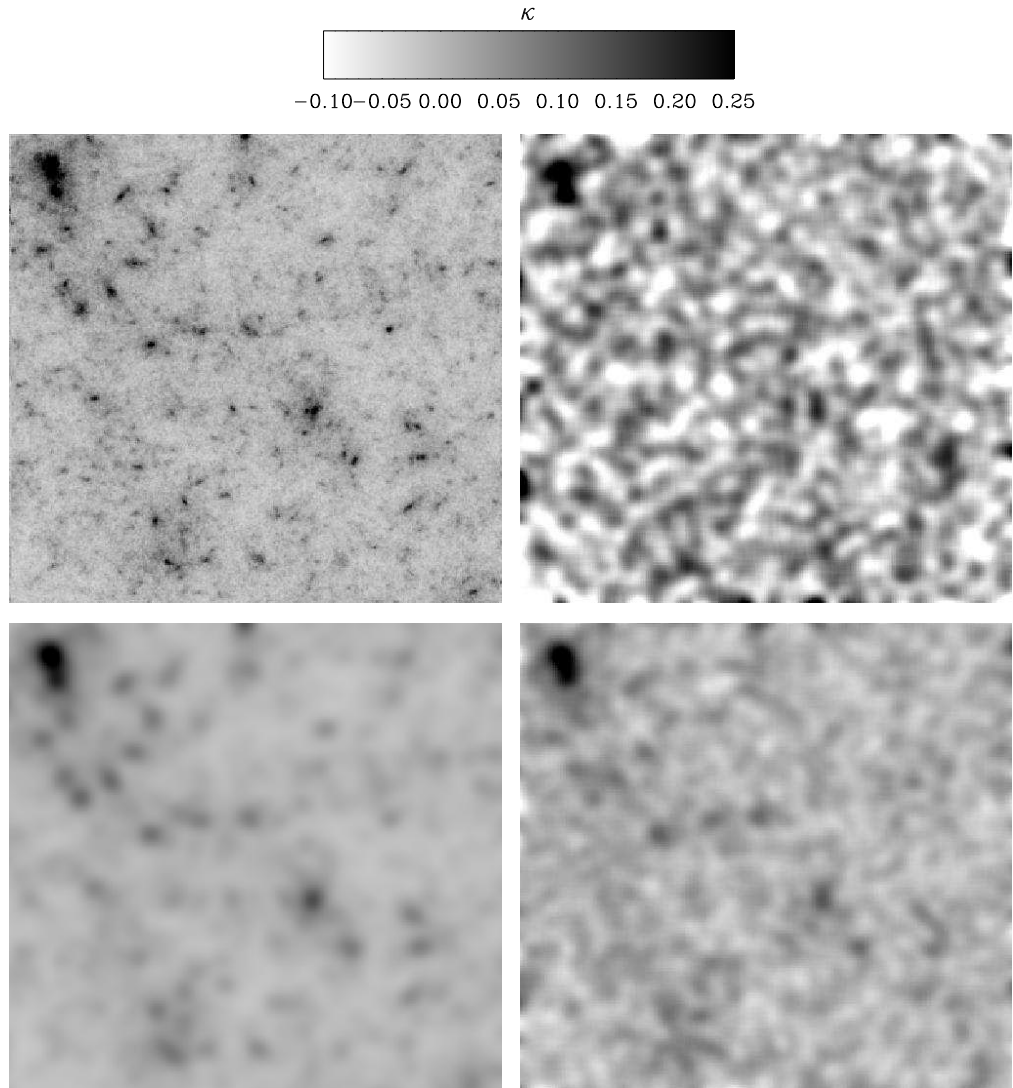


Figure 12. Reconstructed 2-dimensional maps of convergence κ , each $30' \times 30'$. Convergence is proportional to the total matter density along the line of sight, and can be deduced from the shear field. Top-left: simulated (noise-free) convergence map derived by raytracing through an SCDM N-body simulations of large-scale structure from Jain, Seljak & White (2000), in which the sources are assumed to lie at $z = 1$. Bottom-left: same map but smoothed with a Gaussian kernel with a FWHM of 1 arcmin. Top-right: Reconstruction of the convergence map with a noise realization corresponding to ground-based observations. Statistics are taken from a WHT survey by Bacon *et al.* 2002 ($n_g = 25 \text{ arcmin}^{-2}$ and $\sigma_\gamma = 0.39$). Bottom-right: convergence map with much-improved recovery from the expected noise properties of the SNAP wide survey (*i.e.* $n_g = 105 \text{ arcmin}^{-2}$ and $\sigma_\gamma = 0.31$).

the depth of the HDF, the SNAP deep survey will exceed even this density requirement by a factor of three or four (Massey *et al.* 2004b). Thus, SNAP will open up a new regime of dark matter mapping, allowing direct comparison to be made between mass and light on fine scales over a very wide field of view.

In figure 12 we demonstrate the precision with which SNAP will be able to map the dark matter in an SCDM simulation from Jain, Seljak & White (2000). In this simulation, the source galaxies are assumed to lie on a single plane at $z = 1$. Whilst only the most massive overdensities can be distinguished in ground-based shear data, the recovery is much improved from space. This is mainly due to the three- to four-fold increase in number density of resolved galaxies in even the SNAP wide survey. The statistical correlation of such maps will allow the bias between mass and light to be examined to high accuracy over a large range of scales.

Furthermore, simultaneously combining shear estimation with photometric redshifts will permit the use of a recently formulated direct 3D lensing inversion (Taylor 2001; Heavens in this volume). This method directly recovers the full 3D mass distribution without the need to slice projected maps into redshift bins. Applied to the SNAP deep survey, this technique will detect mass overdensities with a 1σ sensitivity lower than $10^{13}M_{\odot}$ at $z = 0.25$. An unbiased, mass-selected cluster catalogue will trace the growth of mass structures in the universe (see Miyazaki *et al.* 2002 and references therein).

10. Conclusions

A space-based, wide-field imager is ideal for weak lensing measurements. Indeed, a systematic floor due to atmospheric seeing will be reached in the next generation of lensing surveys. This is due both to the isotropic PSF smearing that reduces the number of resolved galaxies for which shape measurements are possible; and anisotropic smearing which cannot be perfectly corrected when it varies from one exposure to the next. The proposed SNAP satellite will have both the wide field needed to survey large, representative cosmic volumes and the low level of instrumental systematics affecting galaxy shapes.

Through a dual wide and deep survey strategy, weak lensing with SNAP will be able to produce unique maps of the dark matter distribution, on small scales and in both 2D and 3D. Weak lensing with SNAP will be able to produce mass-selected cluster catalogues to a 1σ detection threshold of $10^{13}M_{\odot}$ at $z = 0.25$.

Weak lensing primarily measures the distribution of the dark matter, but it is also a powerful probe of dark energy. A change in the equation of state w of dark energy modifies the growth rate of structures and the angular-diameter distance. The resulting changes in the cosmic shear statistics will be easily detectable with future weak lensing surveys. In particular, weak lensing measurements with SNAP will be able to independently constrain cosmological parameters Ω_M , σ_8 and w at a level comparable with and somewhat orthogonal to those from future supernova searches and CMB experiments.

Acknowledgments. The authors would like to thank David Valls-Gabaud and Jean-Paul Kneib for organising a fine winter school. We thank the SNAP weak lensing working group, especially Richard Ellis, for our on-going collaboration and useful discussions.

References

- Bacon, D., Refregier, A., Clowe, D. & Ellis, R. 2001, *MNRAS*, **325**, 1065
 Bacon, D., Massey, R., Ellis, R. & Refregier, A. 2003 *MNRAS* in press, preprint astro-ph/0203134
 Bartelmann, M., & Schneider, P. 1999, astro-ph/9912508
 Benabed, K., & Bernardeau, F. 2001, *Phys. Rev. D*, **64**, 083501
 Benabed, K., & van Waerbeke, L. 2003, astro-ph/0306033
 Bernardeau, F., van Waerbeke, L. & Mellier, Y. 1997, *A&A*, **322**, 1
 Bernardeau, F., van Waerbeke, L. & Mellier, Y. 2002, *A&A*, **389**, 28
 Clowe, D., Trentham, N. & Tonry, J. 2001, *A&A*, **369**, 16
 Dahle, H. *et al.* 2002, *ApJ*, **139**, 313
 Erben, T., van Waerbeke, L., Bertin, E., Mellier, Y. & Schneider, P. 2001, *A&A*, **366**, 717
 Jarvis, M. *et al.* 2003, *AJ*, **125**, 1014
 Jain, B., Seljak, U. & White, S. 2000, *ApJ*, **530**, 547
 Hamana, T. *et al.* 2002, submitted to *ApJ*, preprint astro-ph/0210450
 Hoekstra H, Yee HKC, Gladders M. 2002b. astro-ph/0205205
 Hu, W. 2001, *Phys. Rev. D*, **66**, 3515
 Hu, W., & Tegmark, M. 1999, *ApJ*, **514**, L65
 Hui, L. 1999, *ApJ*, **519**, 9
 Huterer, D. 2001, *Phys. Rev. D*, **65**, 063001
 Huterer, D. & White, M. 2002, *ApJ*, **578**, L95
 Kaiser, N., Squires, G. & Broadhurst, T. 1995, *ApJ*, 449, 460
 Kaiser, N., Tonry, J. & Luppino, G. 2000. *PASP* 112:768. *Pan-STARRS webpage* <http://pan-starrs.ifa.hawaii.edu/>
 Lilly, S. *et al.* 1996, *ApJ*, **455**, 108
 Ma, C.-P., Caldwell, R.R., Bode, P., & Wang, L. 1999, *ApJ*, **521**, L1
 Massey, R. *et al.* 2004a, *MNRAS* 348, 214
 Massey, R. *et al.* 2004b, *AJ* in press, preprint astro-ph/0304418
 Mellier, Y., 1999, *ARA&A*, **37**, 127
 Mellier, Y. *et al.* 2001, Cosmic shear surveys. *Deep Fields, Proc. Eur. South. Obs.*, Oct., *Garching*, Ger. astro-ph/0101130
 Miyazaki, S. *et al.* 2002, *ApJ*, **580**, L97
 Munshi, D., & Wang, Y. 2003, *ApJ*, **583**, 566
 Peacock, J., & Dodds 1996, *MNRAS*, **280**, L19
 Perlmutter, S. *et al.* 1999, *ApJ*, 517, 565

- Perlmutter, S. *et al.* 2003, *SNAP homepage* <http://snap.lbl.gov>
- Pierpaoli, E., Scott, D. & White, M. 2001, *MNRAS*, **325**, 77
- Refregier, A. 2003a, *MNRAS*, **338**, 35
- Refregier, A. 2003b, *ARA&A*, **41**, 645, astro-ph/0307212
- Refregier, A. & Bacon, D. 2003, *MNRAS*, **338**, 48
- Refregier, A. *et al.* 2004, *AJ* in press, preprint astro-ph/0304419
- Rhodes, J., Refregier, A. & Groth, E.J. 2000, *ApJ*, **536**, 79
- Rhodes, J. *et al.* 2004, *Astropart. Phys.* 20, 377
- Spergel, D. *et al.* 2003, submitted to *ApJ*, preprint astro-ph/0302209
- Taylor, A. 2001, *Phys. Rev. Lett.* submitted, preprint astro-ph/0111605
- Tyson, J., Wittman, D., Hennawi, J. & Spergel, D. 2002. *Proc. 5th Int. UCLA Symp. Sources Detect. Dark Matter*, Feb., Marina del Rey, ed. D Cline. astro-ph/0209632, LSST Home Page <http://lsst.org>
- van Waerbeke, L., Hamana, T., Scoccimarro, R., Colombi, S. & Bernardeau, F. 2001, *MNRAS*, **322**, 918
- van Waerbeke, L. *et al.* 2002, submitted to *A&A*, preprint astro-ph/0202503
- Viana, P. & Liddle, A. 1999, *MNRAS*, **303**, 535
- Weinberg, N., & Kamionkowski, M., 2002, submitted to *MNRAS*, preprint astro-ph/0210134
- Williams, R. *et al.* 1996, *AJ*, **112**, 1335
- Williams, R. *et al.* 1998, *A&AS*, **193**, 7501
- Wittman DM. 2002. *Dark Matter and Gravitational Lensing, LNP Top. Vol.*, ed. F Courbin, D Minniti. Springer-Verlag. astro-ph/0208063